

Chapter 10

Numerical Simulation of the Plasma Inside a Glow Discharge Millimeter Wave Detector



Cemre Kusoglu-Sarikaya, Demiral Akbar and Hakan Altan

Abstract Nowadays, Terahertz (THz) and mm-waves are encountered in many branches such as security, industry and medicine. However, limitations in existing commercial detectors in terms of cost, speed and responsivity prevent this highly advantageous region of the electromagnetic spectrum from being used more efficiently. For these reasons, neon indicator lamps, otherwise known as glow discharge detectors (GDDs), have succeeded in attracting the attention of researchers, not only because they are cheap, but also because of their better performance to other technologies. In these detectors, detection occurs as a result of the interaction of THz/mm-wave with the plasma in the lamp. Although this interaction has been tried to be explained qualitatively using various analytical models, there has been no accurate quantitative explanation about this interaction in the literature. The problem is mainly due to the confined plasma environment which can be difficult to resolve with equilibrium models. As known, GDDs are non-local thermal equilibrium plasma lamps, and such plasmas need to be modeled with a kinetic approach. For that reason, in this study, parallel 1d3v Particle in Cell/Monte Carlo Collision (PIC/MCC) simulation of the plasma in the neon lamp is performed. This simulation will form the basis for the planned investigations into understanding the effects of THz/mm-waves on the plasma. The kinetic approach employed in the simulation allows us to accurately understand and predict the plasma parameters causing the glow discharge in GDDs. The results are checked using experiments performed on home-built discharge glow chambers with similar gap dimensions.

C. Kusoglu-Sarikaya (✉) · H. Altan
Middle East Technical University, Department of Physics, 06800 Ankara, Turkey
e-mail: ckusoglu@metu.edu.tr

H. Altan
e-mail: haltan@metu.edu.tr

D. Akbar
Department of Mechanical Engineering, Ostim Technical University, 06370 Ankara, Turkey
e-mail: demiral.akbar@ostimteknik.edu.tr

10.1 Introduction

Although THz and mm-waves can be used in many areas, the lack of a cheap, fast and room-temperature detection mechanisms limits the usability of these waves. For these reasons, it is of great importance to investigate the usability of GDDs for THz and mm-wave detection since they are fast (less than 1 μ s rise time), simple, cheap and they can operate at room temperature [1]. In addition, recent studies [2, 3] have yielded promising results. When compared with the commercial detectors available today, it was observed that although glow discharge detectors have the same performance as pyroelectric detectors, Golay cells, bolometers and Schottky diodes, GDDs are better in terms of speed and response time [2, 4]. Also, the fact that GDDs are relatively cheap gives them a great advantage over all of these other expensive detectors.

Detectability of electromagnetic radiation using dc gas discharge plasmas began to be explored by researchers in the 1950s as a result of Burroughs and Bronwell's observation [5] of changes in the discharge current caused by absorption of microwave radiation. After this observation, although the detectability of microwave radiation in different glow discharge regions was investigated [6, 7] and an attempt was made to explain the detection mechanism [8, 9], a definite conclusion was not reached. While Lobov [8] argued that diffusion current could occur as a result of the absorption of microwave radiation, Severin [9] suggested that the absorbed radiation energy could cause a reduction in the ionization potential.

The usability of indicator lamps as microwave radiation detectors was firstly investigated by Farhat [10]. Meanwhile, Severin [9, 11] showed that millimeter wave frequencies can also be detected using glow discharge plasma. Later, Kopeika [12] observed in his studies that the spectral response ranges of GDDs began at microwave and extended to x-ray. GDD's detection mechanism is activated by interaction of plasma in the lamps with mm-wave or THz radiation. Since the frequency of the plasma is in the sub-GHz to GHz range, such waves can penetrate into the plasma. Taking into account the theories previously made for the mechanism of interaction between microwave and plasma [8, 9], Kopeika [13] demonstrated under what conditions enhanced diffusion and enhanced ionization occur. Although all works done so far to explain the interaction mechanism has given an idea about this mechanism, they cannot precisely explain the physical events that took place during the interaction. For this reason, in this study, the plasma in GDD was simulated using the parallel 1d3v PIC/MCC code [14]. By using this simulation, the aim here is to understand the basic plasma parameters such as eedf, iedf, ion and electron densities, the electric field and potential that cause the expected normal and abnormal glow discharge in these lamps. For a better understanding of the simulation results, a brief description of the gas discharge plasma will be given in the following section. Then, the question of why their use with THz and mm-waves attract so much attention will be tried to be answered in Sect. 10.3. In Sect. 10.4, glow discharge detectors which have many promising features in terms of detection of these radiations will be mentioned. Then, after the validation of the code in Sect. 10.5, the procedures followed for simulating

these GDDs will be described in Sect. 10.6. Finally, the simulation results will be discussed in Sects. 10.7 and 10.8.

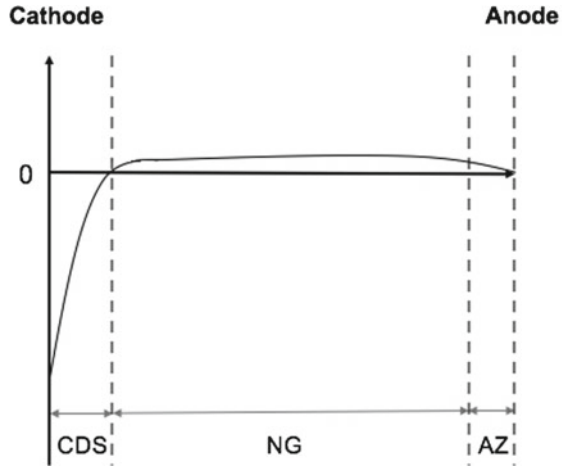
10.2 Gas Discharge Plasmas

Gas discharge plasmas occur when an electric current flows through the plasma or when the electromagnetic radiation is absorbed by the plasma. The best known example of discharge in nature is lightning. Due to their thermodynamic properties, discharges can be classified into two types: local thermal equilibrium (LTE) and non local thermal equilibrium (non-LTE) discharges. In LTE, all plasma particles are at the same temperature, while in non-LTE, which is the scope of this chapter, the temperature of electrons is much higher than that of other plasma particles. In fact, this can be explained by pressure. At high gas pressure ($10\text{--}10^3$ kPa), there are too many collisions in the plasma, resulting in efficient energy exchange. As a result, the plasma particles will have equal temperatures. On the contrary, different temperature values will be observed in the plasma particles at low gas pressure ($10^{-4}\text{--}1$ kPa) since there will be a few collisions and consequently no efficient energy exchange between the particles.

Gas discharge plasmas can also be formed in laboratories using sources such as direct current (dc), capacitively coupled radio frequency (rf), inductively coupled rf and microwaves [15, 16]. These sources vary according to the application to be used. Today, many technological applications, such as surface modification [16, 17], ozone generation [18], plasma thrusters and rocket propulsion [19], use gas discharge plasmas. Especially in light production systems such as in lamps [20] and in plasma displays [21], they are used efficiently.

In this study, we will focus on the dc glow discharges that occur in GDDs. The regions formed in such discharges are summarized in Fig. 10.1. It can be seen that although the applied potential difference between the anode and the cathode is constant in dc glow discharge, the potential and the electric field are not uniformly distributed between the electrodes. In the region next to the cathode, called the cathode dark space (CDS), the potential drops rapidly almost to zero and this drop causes a strong electric field. This region is also called the sheath region. After a sudden drop, the potential remains almost constant in the area called the negative glow (NG). Finally, the potential returns to zero in the anode zone (AZ). When the inter-electrode distance is longer, two separate regions called Faraday dark space (FDS) and positive column (PC) emerge. The negative electric field in these regions, provides the electrons move toward the anode. Since the distance between the electrodes is about 1 mm, these regions are not formed in GDDs. The lamps having an inter-electrode distance of 1–2 mm, have only one glow region close to the cathode and most likely this region can be characterized as the negative glow [22].

Fig. 10.1 The dc glow discharge regions at short inter-electrode distance and/or low pressure



10.3 THz and MM-Waves

It is known that the majority of the universe is filled with mm-wave and THz energy (0.123–12.3 meV), although it has a low enough energy to be detected [23]. This energy value falls in the range of 1.43–143 K, which is considerably lower than the earth's ambient background temperature. This type of energy is mostly emitted from cold dust in the interstellar environment [24]. MM-waves, are in the range of 30–300 GHz in the electromagnetic spectrum, right next to the THz waves (300 GHz–3 THz). As the name implies, the wavelengths of these waves are in millimeter order. The presence of resonant absorption of THz/mm-waves in water and oxygen molecules limits their usability in long distance communications [25]. However, they can be used in many applications at distances of about 10m [26]. In addition, their short wavelengths allow to transmit a lot of data at one time.

Since THz and mm-waves have a wide variety of properties, it is possible to use them in many areas. First of all, these waves are very beneficial in the field of security [27, 28] because they can penetrate many non-conductive materials and high resolution images can be obtained due to their short wavelengths. In addition, the presence of characteristic spectra of some explosives at the THz frequency gives them a great advantage in terms of detection as well as identification. As known, THz/mm waves are non-ionizing radiations and can be used on humans. With this feature, it has been found that these radiations can also be used in pharmaceutical [29, 30], medical [31, 32] and non-destructive testing areas [33].

Despite all these advantageous features, the available sources and detectors for THz/mm-waves are quite limited. In particular, the fact that existing commercial detectors are very expensive restricts the efficient use of these waves. For this reason, in this study, GDDs with a cheap and promising THz/mm-wave detection mechanism is tried to be understood by examining the parameters of the plasma formed inside them.

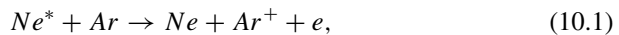
10.4 Glow Discharge Detectors

Some of the more common, currently available commercial detectors for THz/mm-waves are Schottky diodes, Golay cells, pyroelectric detectors and bolometers [23]. The investigations [2–4] have shown that GDDs are more advantageous than these detectors because they are cheap, fast and operate at room temperature. They also show relatively low sensitivity to changes in ambient temperature [9, 11, 35].

GDDs are glass tubes containing two electrodes and a low-pressure noble gas, some have a phosphorescent coating inside the glass. A sufficient potential difference between the electrodes causes the ionization of the gas and thus the formation of electrons and ions. As the negatively charged particles move toward the anode, the positively charged particles move toward the cathode, causing secondary electron emission in the cathode, which plays an important role in the sustainability of the generated plasma. The light is the result of excitation of the gas atoms by the electrons in the plasma. The excited gas atoms fall to a lower energy level by emitting photons in a color that is characteristic of the gas.

Different noble gases can be used in GDDs. Since each gas has different characteristics such as molecular weight and ionization energy, the plasma parameters of GDDs using different noble gases are different. This difference affects the THz/mm-wave detectability [38]. The lowest efficiency from GDD is obtained when helium gas is used. Since the ionization energy of helium is the highest among the noble gases, the discharge potential of this gas is also the highest. As a result, the electric field will be higher than the THz/mm-wave electric field, so the radiation effect will not be observed efficiently. Although argon, krypton, and xenon gases have lower ionization energies, they require a higher discharge potential to reach the cathode and form secondary electrons, since they are heavier. This, as mentioned for the helium gas, reduces the efficiency of the detector. Neon gas with low atomic weight has the lowest discharge potential, which leads to the ability to detect THz/mm-waves with the greatest responsivity [38].

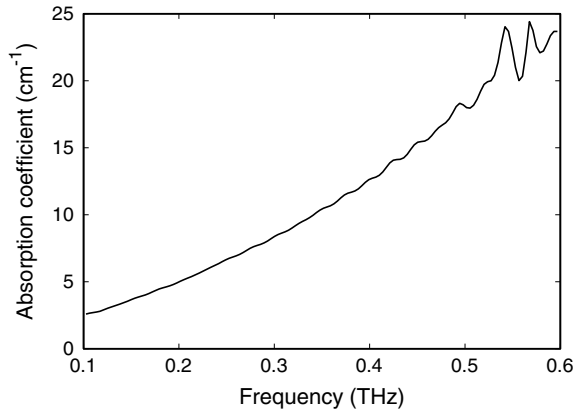
In GDDs, noble gases can be used in mixture form as well as in pure form. Generally, Ne-Ar mixture is used to reduce the discharge potential of the neon gas to lower values. Since the excited neon atoms have higher energy than the ionization energy of argon gas, excited neon atoms can ionize the argon gas. The reaction, which has the form



is called Penning ionization. With this reaction, ionization can occur at lower voltage values [39]. In Ne-Ar mixture, when 1 or less percent of argon gas is used, Penning ionization occurs at a significant level. However, when the percentage of argon gas is further increased, the argon gas will begin to be ionized directly by the electrons, thus the effect of Penning ionization will be reduced [40].

In GDDs, as well as the gas used, the operation in different dc glow discharge regions affects THz/mm-wave detection. In the Townsend region, a large amount of photons are needed for THz/mm-wave detection, since electrons mostly have low

Fig. 10.2 Absorption coefficient of the glass wall typically used in a commercial GDD



energy. In the subnormal glow region, discharge current is very low and mainly caused by ion-induced secondary electron emission in the cathode. For that reason, the main contribution to the noise comes from this secondary emission process [41, 42]. It is not appropriate to work in this region because this noise will cover the THz/mm-wave signal [25]. In the arc discharge region, it is very difficult for GDDs to work stably since large amounts of thermal noise will occur. GDDs need to be operated in normal or abnormal glow regions in order to detect THz/mm-waves efficiently. Because, in these regions, the discharge current is the result of both ion-induced secondary electron emissions and electron-neutral collisions. As a result of the interaction of THz/mm-waves with the electrons, the increase in energy of the electrons will affect electron-neutral collisions and therefore cause a change in the discharge current.

Since the frequency of the THz/mm-waves is greater than the plasma frequency (in the sub-GHz to GHz range [1, 43]), these waves can pass through the plasma in neon lamps. It is thought that this interaction results in a change in the discharge current through cascade ionization and diffusion current [13]. Cascade ionization is the process by which electrons ionize neutrals in a shorter time with the energy they absorb from electromagnetic waves. This event results in an increase in the discharge current. Diffusion current is, however, the fact that electrons diffuse into the electrodes without performing ionization with the energy they absorb, and this diffusion causes a decrease in the discharge current. Both of these events are thought to occur during the interaction with plasma in the GDDs, but one dominates [13]. Indeed, in some studies with GDD, it was observed that the discharge current increased after interaction [1, 13], whereas in the other studies it was observed that the discharge current had decreased [2]. Although these studies have made a great contribution to the understanding of GDDs, they have been limited to analytical models and qualitative explanations. It is still unclear what kind of physical events take place during the interaction of THz/mm-wave and plasma.

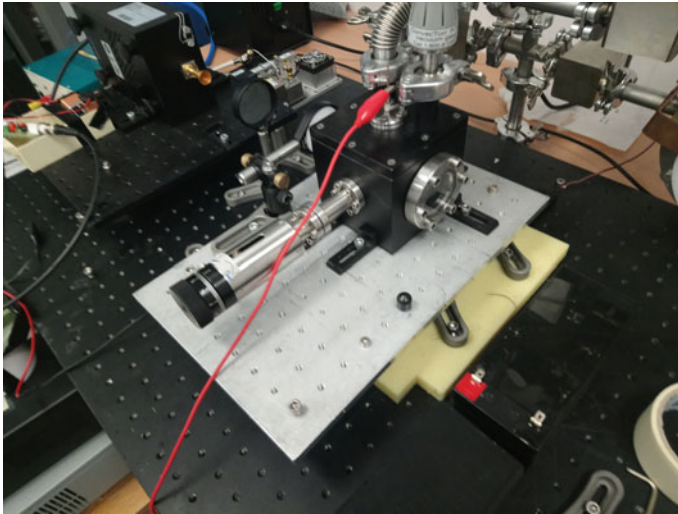


Fig. 10.3 Plasma discharge chamber. The chamber can be filled by a single or mixture of gases. The distance between the anode and cathode can be adjusted with $10\ \mu\text{m}$ precision

In addition, since neon lamps are not designed as detectors, they have to be optimized. For example, in Fig. 10.2, the absorption coefficient of the glass wall of the GDDs is plotted according to the frequency. As can be seen, there is a significant loss in power of the THz wave after the glass wall. First of all, a different material must be used in order to prevent this loss. Furthermore, since the distance between the electrodes affects the plasma, determining the optimum value of this distance is of great importance. For this reason, the plasma discharge chamber shown in Fig. 10.3 has been developed in our laboratory to determine the optimum parameters required for the use of GDDs as detectors. The dimension of this chamber is $10 \times 10 \times 10\ \text{cm}^3$. It has two quartz windows with a diameter of 40 mm which allow the transmission of THz radiation. The inter-electrode distance can be increased to 2 cm with $10\ \mu\text{m}$ resolution. With two feedthroughs on the top of the chamber, instantaneous pressure measurement and distribution of gas mixtures can be made. Up to three different gases can be mixed with the gas mixer system. Also, the rotary vane pump allows the pressure in the chamber to be reduced to 10^{-2} torr. To be able to use this chamber to find the optimum parameters efficiently, it is first necessary to understand the plasma parameters in GDDs and the effects of these parameters on the THz/mm-wave and plasma interaction. For this purpose, in this study, the parallel 1d3v PIC/MCC code [14] is used to compute the basic plasma parameters such as eedf, iedf, ion and electron densities, the electric field and potential inside the GDD.

10.5 Validation of the PIC/MCC Simulation Code

As known, GDDs are low pressure non-LTE plasma lamps. For this reason, as mentioned in Sect. 10.2, since the energy exchange is not done efficiently in these type of plasmas, the plasma particles do not have the same temperature. In order to understand the behavior of such plasma particles adequately, a kinetic approach is required. This approach can be obtained by using the distribution function $f(\mathbf{r}, \mathbf{v}, t)$ defined by the Boltzmann equation,

$$\left[\frac{\partial}{\partial t} + \mathbf{v} \nabla_{\mathbf{r}} + \mathbf{a} \nabla_{\mathbf{v}} \right] f(\mathbf{r}, \mathbf{v}, t) = \left(\frac{\partial f}{\partial t} \right)_{\text{coll.}}, \quad (10.2)$$

where, \mathbf{v} , \mathbf{r} and \mathbf{a} are the velocity, position and acceleration of the plasma particles, respectively. However, since the direct solution of this equation is highly complicated mathematically, particle simulation methods that give the same results [44, 45] can be used to explain the kinetic behavior of particles. One of these methods is the well-known PIC/MCC method. In this study, the plasma in the GDD is simulated using the parallel 1d3v PIC/MCC code [14]. The code is written in Fortran 90 language and parallelized by using Open MPI library for performance enhancement. However, since the gas pressure and the gas mixture ratios (if gas mixture is used) used in neon indicator lamp are not known exactly, before simulating GDDs, an experiment was performed with argon gas in the home built chamber with certain parameters and the discharge current obtained from the experiment is compared with that obtained from the simulation. Inside the chamber, the argon gas pressure is held constant at 1.7 torr and the background pressure is reduced to about 0.01 torr. The distance between the electrodes is set to be 1.2 mm.

As can be seen from Fig. 10.4, under the specified conditions, when 350 V is applied to the argon gas, a discharge current of 0.38 ± 0.04 mA is obtained. Taking this result into consideration, the experiment is simulated. The types of collisions

Fig. 10.4 The voltage-current characteristic obtained for argon gas in the plasma discharge chamber

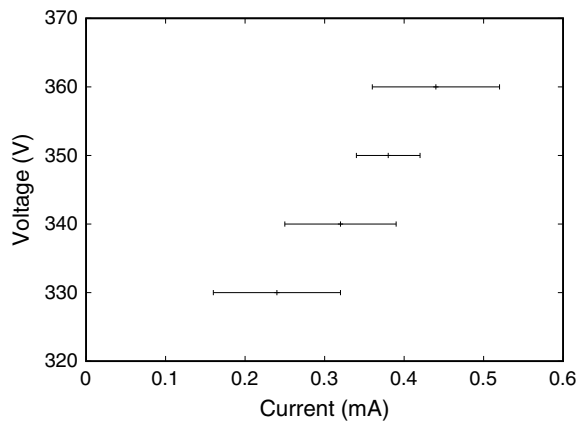


Fig. 10.5 Elastic, excitation, ionization cross-section curves for electrons in argon gas. These data were taken from [46]

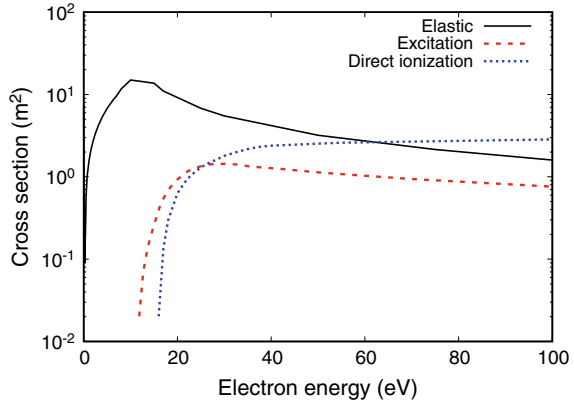


Fig. 10.6 Isotropic and backward scattering cross-section curves for ions in argon gas. These data were taken from [47]

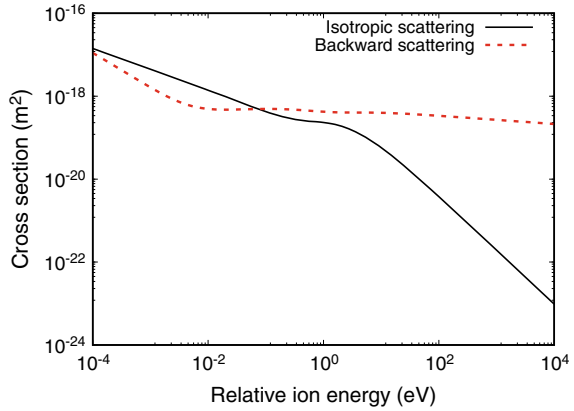


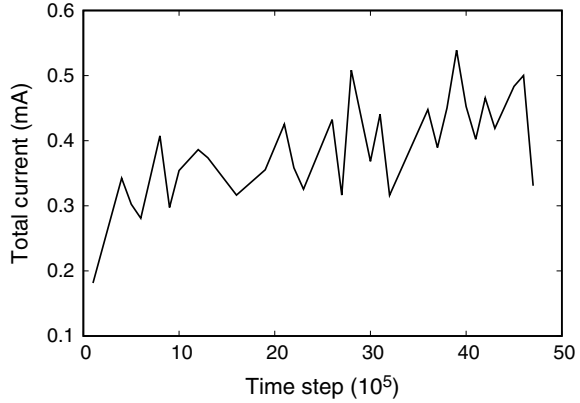
Table 10.1 The numerical parameters used in the PIC/MCC simulation of argon gas

Weighting (10 ⁸)	2.4
Grid number	600
Time step (10 ⁻¹² s)	4
Gas temperature (K)	300
Secondary electron emission coefficient (γ)	0.13
Reflection coefficient (r)	0.2

considered in the simulation, and the cross-section curves of these collisions [46, 47] are shown in Figs. 10.5 and 10.6. Numerical parameters used are summarized in Table 10.1.

As a result of the simulation, the total current, which contains the electron, ion and displacement current, is obtained over time (Fig. 10.7). It is apparent that the total current starts to converge around 0.4 mA after the 4×10^6 th time step, which corre-

Fig. 10.7 The change of the total current with time obtained in the simulation of Ar glow discharge. Each time step corresponds to 4×10^{-12} s



sponds to the real time of $16 \mu\text{s}$. This converged result is approximately in agreement with the discharge current obtained from the experiment. This compatibility supports the usability of the code for simulating a commercially available GDD.

10.6 Parallel 1d3v PIC/MCC Simulation of GDD

By using parallel 1d3v PIC/MCC code, GDD is simulated using neon gas and Ne-Ar mixture, separately. Between electrons and neutrals, elastic, excitation and ionization reactions are considered in the code. The cross section curves describing these reactions are shown in Fig. 10.8.

As shown in Fig. 10.8, only excitations to $Ne(^3P_2)$ are considered for the excitation reaction. This is because the metastable atoms at this level are known to be responsible for the Penning ionization of the argon gas [1]. In addition, in order to

Fig. 10.8 Elastic, excitation, ionization cross-section curves for electrons in neon gas. These data was taken from [48]

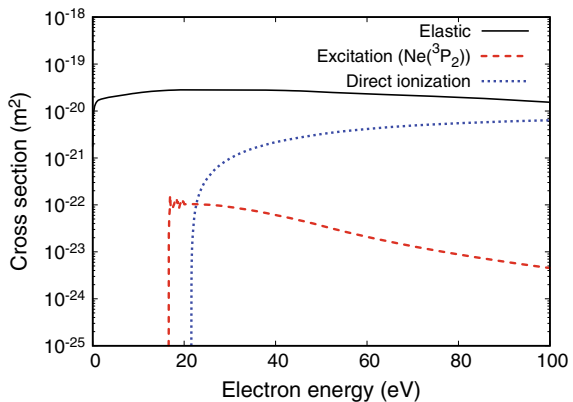


Table 10.2 The physical and numerical parameters used in the GDD simulation

Weighting (10^8)	2.6
Grid number	600
Time step (10^{-12} s)	4
Distance (mm)	1.3
Gas temperature (K)	300
Pressure (torr)	25
Voltage (volt)	115

prevent excessive time consumption in the simulation, the density distribution of excited atoms ($Ne(^3P_2)$) is investigated by using the fluid approximation,

$$\frac{\partial n}{\partial t} - D \frac{\partial^2 n}{\partial x^2} = S, \quad (10.3)$$

where D is the diffusion coefficient taken [49, 50] as $150 \text{ cm}^2\text{s}^{-1}$ torr and S is the excitation source term. This approximation is combined with the PIC/MCC model.

Between ions and neutrals, it is assumed that there are basically two separate reactions: isotropic scattering and charge transfer. Cross-section values for these reactions were taken as 2×10^{-19} and $3 \times 10^{-19} \text{ m}^2$ [51], respectively.

It is well known that the ion-induced secondary electron emission, which occurs in the cathode, plays a major role in the sustainability of the plasma in discharge lamps. This reaction is defined by a secondary electron emission coefficient, γ . In our previous work [52], this coefficient was taken as 0.2, considering that the electrode in the neon lamp is tungsten [53]. However, it is known that coatings on electrodes are used to reduce the work function value in such lamps. In the literature, it is stated that the reduction of around fifty percent is achieved by coatings [54, 55]. For this reason, it would be more reasonable to increase the secondary electron emission coefficient by 50% to 0.3. Other parameters used in the simulation are summarized in Table 10.2.

10.7 Simulation Results (Pure Neon Gas)

Figure 10.9 shows the potential and electric field curves obtained from the simulation by using pure neon gas. As can be seen, the sheath region, where the electric field is strong, is seen between 1 and 1.3 mm. It is also evident that the negative glow region, where the potential is almost constant, covers a very large distance of 0.1–1 mm and no positive column or Faraday dark space regions are observed as expected.

Figure 10.10 shows the distribution of the density of electrons, ions, and excited neon atoms between the electrodes. As can be seen, the maximum density is observed

Fig. 10.9 Electric field and electric potential profiles obtained by using pure neon gas

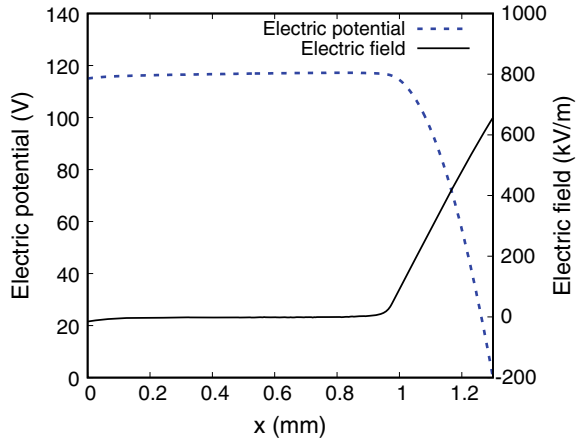


Fig. 10.10 Electron, ion and metastable neon density distribution obtained by using pure neon gas

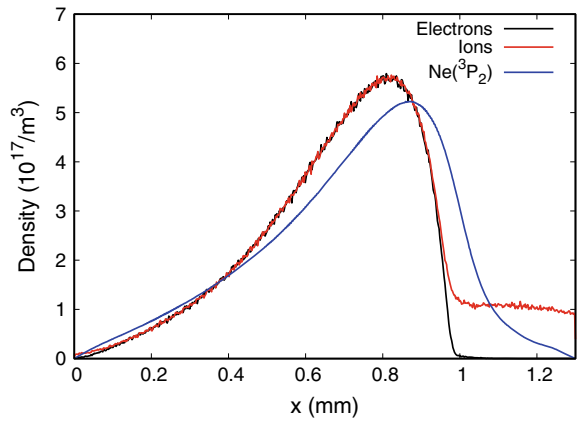
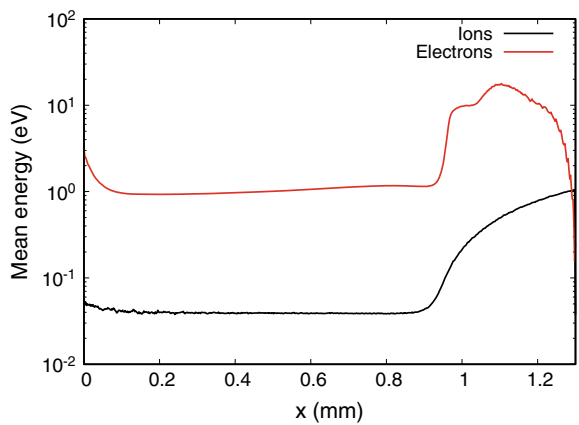


Fig. 10.11 Electron and ion mean energy distribution obtained by using pure neon gas



in a region close to the cathode. This value corresponds to the maximum plasma frequency (f_p) of 7 GHz. This supports the statement in the literature that the plasma frequency in the neon indicator lamps is on the order of a few GHz [1, 43].

The mean energy distributions of electrons and ions are shown in Fig. 10.11. As mentioned in Sect. 10.2, since GDDs are non-LTE plasma lamps, the temperature of electrons is much higher than the temperature of other plasma particles. This is evident in the graph of mean energy distribution. In addition, it is observed that particles are energized by the effect of the strong electric field in the sheath region, as expected. Low energetic particles appear dominantly in the negative glow region where quasi-neutrality is observed. This demonstrates that the particles effectively lose their energy in this region as a result of elastic collisions. Two distinct Maxwellian regions formed by these high and low energetic particles can also be seen in the distribution function profiles (Figs. 10.13 and 10.14). In the region formed by high-energy electrons, a wide peak is observed around 14 eV. By looking at the mean energy graph (Fig. 10.11), it can be seen that the electrons having these energies are

Fig. 10.12 Comparisons of electron densities obtained by using pure Ne and Ne-Ar mixture, separately

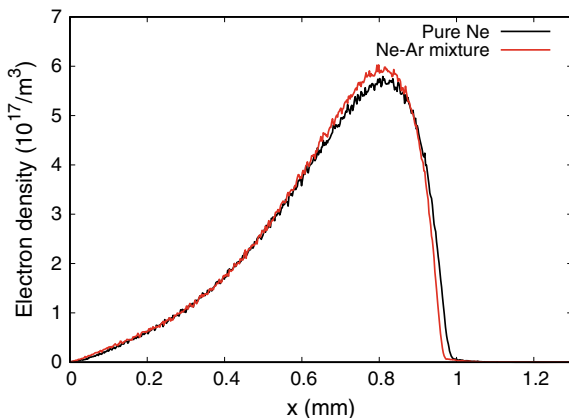


Fig. 10.13 Electron energy distribution function profiles obtained by using pure Ne and Ne-Ar mixture, separately

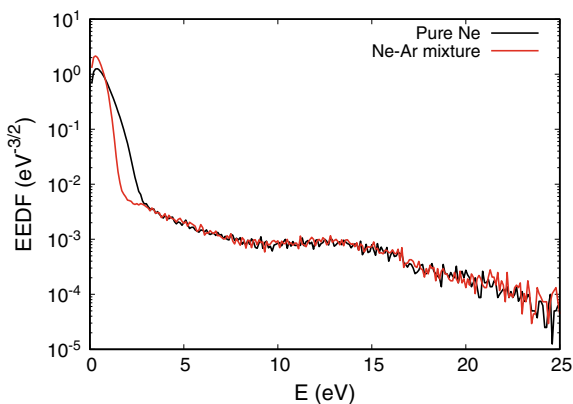
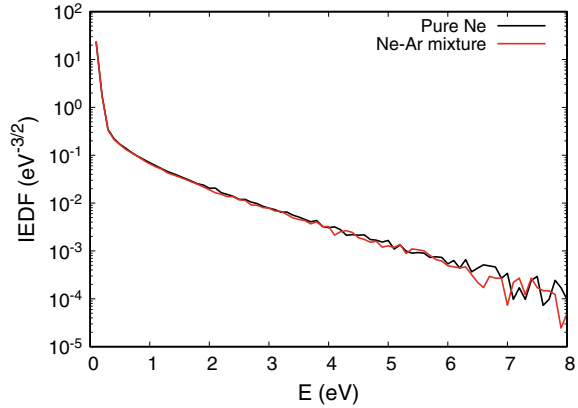


Fig. 10.14 Ion energy distribution function profiles obtained by using pure Ne and Ne-Ar mixture, separately



in a region close to the cathode. In Sect. 10.5, it was stated that the coatings on the electrodes are used to increase the ion-induced secondary electron emission efficiency in the discharge lamps. This ensures that the secondary electron emission is an effective reaction in this type of lamps. For this reason, it is thought that secondary electrons emitted from the cathode accelerate in the strong electric field and form this peak.

10.8 Simulation Results (Ne-Ar Mixture)

The simulation was repeated with the same parameters, adding only 1% argon gas to the neon gas. The electron density graph obtained from this simulation is compared with that obtained when pure neon gas is used (Fig. 10.12). As can be seen, the effect of Penning ionization, which occurs in the Ne-Ar mixture, is confirmed by an increase in density. This increase means that the profile obtained when the mixture is used can be reached with a lower potential difference than when pure neon gas is used. This explains why the gas mixture is preferred in commercial neon indicator lamps. However, since the increase observed here is negligible, it is understood that the percentage of argon should be kept below 1%.

Furthermore, the effect of gas mixture on the energy distribution profiles of the particles are also investigated (Figs. 10.13 and 10.14). While there is no change in the energy distribution of ions, the effect of low energetic electrons emitted by Penning ionization is clearly visible in the energy distribution of electrons at low energies.

10.9 Conclusions

Gas Discharge Detectors (GDDs) offer many advantages over other methods in detection of mm wave and terahertz radiation. While efforts have been made to qualitatively explain the detection mechanism behind commercially available GDDs, the low pressure non-LTE medium inside these lamps can only be truly understood quantitatively using a kinetic approach. Parallel 1d3v PIC/MCC simulation is performed to simulate this plasma medium. Since parameters such as pressure and gas mixture ratio are not known exactly for neon indicator lamp, first, an experiment with a certain pressure and voltage value was performed with a home-built plasma discharge chamber developed in our laboratory. The parallel 1d3v PIC/MCC code is found to be successful in validating the experimental measurements performed when pure argon gas is used as the discharge medium inside this chamber for similar discharge dimensions as in GDDs.

After the validation process, the GDD is simulated by using Ne and Ne-Ar mixture, respectively. First of all, it was observed from the potential and the electric field profile that the negative glow region in GDDs covers most of the inter-electrode distance. Since the distance between the electrodes is approximately 1 mm, positive column and Faraday dark space regions are not observed. Electron and ion density distributions in the negative glow region show that the plasma frequency, f_p , is in the GHz range, as indicated in the literature. Furthermore, the observed differences in the mean energy of the plasma species are in accordance with the characteristics of the non-LTE plasmas. Finally, the increase in density obtained when Ne-Ar mixture is used shows that the use of this mixture causes a decrease in the breakdown voltage. This explains why gas mixtures are preferred in commercial GDDs. However, it has been observed that the Penning effect is negligible for the percentage of argon gas used in this simulation.

In conclusion, it has been shown that the PIC/MCC simulation is useful for quantitatively determining the plasma properties of GDDs. This tool will further allow one to investigate the plasma-THz/mm-wave interaction where it is thought that the radiation increases the collisions inside the plasma and where an increase in detection is observed when the GDD is operated in the abnormal glow regime. Quantizing this interaction will allow one to better design and optimize the detection inside the glow discharge detector.

Acknowledgements The work was supported by the Scientific and Technical Research Council of Turkey (TUBITAK) 115F226. This research is also sponsored in part by the NATO Science for Peace and Security Programme under grant MD.SFPP 984775. The simulations were performed using High Performance and Grid Computing Center (TRUBA Resources) at TUBITAK ULAKBIM.

References

1. N.S. Kopeika, Glow discharge detection of long wavelength electromagnetic radiation: cascade ionization process internal signal gain and temporal and spectral response properties. *IEEE Trans. Plasma Sci.* **6**, 139–157 (1978)
2. A. Abramovich, N.S. Kopeika, D. Rozban, E. Farber, Inexpensive detector for terahertz imaging. *Appl. Opt.* **46**, 7207–7211 (2007)
3. A. Abramovich, N.S. Kopeika, D. Rozban, E. Farber, Terahertz detection mechanism of inexpensive sensitive glow discharge detector. *J. Appl. Phys.* **103**, 093306 (2008)
4. L. Hou, W. Shi, Fast terahertz continuous-wave detector based on weakly ionized plasma. *IEEE Electron Device Lett.* **33**, 1583–1585 (2012)
5. C. Burroughs, A. Bronwell, *Teleteknik* **II**, 62 (1952)
6. M.A. Lampert, A.D. White, Microwave techniques for studying discharges in gases. *Electron. Commun.* **30**, 124–128 (1953)
7. B.J. Udelson, Effect of microwave signals incident upon different regions of a dc hydrogen glow discharge. *J. Appl. Phys.* **28**, 380–381 (1957)
8. G.D. Lobov, Gas discharge detector of microwave oscillations. *Radiotekh. Electron.* **5**, 152–165 (1960)
9. P.J.W. Severin, *The Interaction of Microwaves with the Cathode Fall and Negative Glow in a Glow Discharge* (Philips Research Laboratories, Eindhoven, Netherlands, 1965)
10. N.H. Farhat, A plasma microwave power density detector. *Proc. IEEE* **52**, 1053–1054 (1964)
11. P.J.W. Severin, A.G. Van Nie, A Simple and rugged wide-band gas discharge detector for millimeter waves. *IEEE Trans. Microw. Theory Tech.* **14**, 431–436 (1966)
12. N.S. Kopeika, Theory of a fast, sensitive, submillimeter wave glow discharge detector. *Int. J. Infrared Millim. Waves* **5**, 1333–1348 (1984)
13. N.S. Kopeika, On the mechanism of glow discharge detection of microwave and millimeter-wave radiation. *Proc. IEEE* **63**, 981–982 (1975)
14. C. Kusoglu-Sarikaya, I. Rafatov, A.A. Kudryavtsev, Particle in cell/Monte Carlo collision analysis of the problem of identification of impurities in the gas by the plasma electron spectroscopy method. *Phys. Plasmas* **23**, 063524 (2016)
15. A. Bogaerts, E. Neyts, R. Gijbels, J.V.D. Mullen, Gas discharge plasmas and their applications. *Spectrochim. Acta B* **57**, 609–658 (2002)
16. M.A. Lieberman, A.J. Lichtenberg, *Principles of Plasma Discharges and Materials Processing* (Wiley, New York, 1994)
17. A. Grill, *Cold Plasma in Materials Fabrication: From Fundamentals to Applications* (IEEE Press, New York, 1994)
18. T. Hammer, Applications of plasma technology in environmental techniques. *Contrib. Plasma Phys.* **39**, 441–462 (1999)
19. D.M. Goebel, I. Katz, *Fundamental of Electric Propulsion: Ion and Hall Thrusters* (Wiley, New Jersey, 2008)
20. J.R. Coatan, A.M. Marsden, *Lamps and Lightning* (Arnold, London, 1997)
21. A. Sobel, Plasma displays. *IEEE Trans. Plasma Sci.* **19**, 1032–1047 (1991)
22. N.S. Kopeika, J. Rosenbaum, R. Kastner, Abnormal glow discharge detection of visible radiation. *Appl. Opt.* **15**, 1610–1615 (1976)
23. P.H. Siegel, Terahertz technology. *IEEE Trans. Microw. Theory Tech.* **50**, 910–928 (2002)
24. D.T. Leisawitz, W.C. Danchi, M.J. DiPirro, L.D. Feinberg, D.Y. Gezari, M. Hagopian, W.D. Langer, J.C. Mather, S.H. Moseley, M. Shao, R.F. Silverberg, J.G. Staguahn, M.R. Swain, H.W. Yorke, X. Zhang, Scientific motivation and technology requirements for the SPIRIT and SPECS far-infrared/submillimeter space interferometers. *Proc. SPIE* **4013**, 36–46 (2000)
25. L. Hou, H. Park, X. Zhang, Terahertz wave imaging system based on glow discharge detector. *IEEE J. Sel. Top. Quant.* **17**, 177–182 (2011)
26. T.S. Hartwick, D.T. Hodges, D.H. Barker, F.B. Foote, Far infrared imagery. *Appl. Opt.* **15**, 1919–1922 (1976)

27. M.C. Kemp, P.F. Taday, B.E. Cole, J.A. Cluff, A.J. Fitzgerald, W.R. Tribe, Security applications of terahertz technology. *Proc. SPIE* **5070**, 44–52 (2003)
28. W.R. Tribe, D.A. Newnham, P.F. Taday, M.C. Kemp, Hidden object detection: security applications of terahertz technology. *Proc. SPIE* **5354**, 168–176 (2004)
29. P.F. Taday, Applications of terahertz spectroscopy to pharmaceutical sciences. *Philos. Trans. R. Soc. London Ser. A* **362**, 351–364 (2004)
30. C.F. Strachan, P.F. Taday, D.A. Newnham, K.C. Gordon, J.A. Zeitler, M. Pepper, T. Rades, Using terahertz pulsed spectroscopy to quantify pharmaceutical polymorphism and crystallinity. *J. Pharm. Sci.* **94**, 837–846 (2005)
31. E. Pickwell, B.E. Cole, A.J. Fitzgerald, M. Pepper, V.P. Wallace, In vivo study of human skin using pulsed terahertz radiation. *Phys. Med. Biol.* **49**, 1595–1607 (2004)
32. V.P. Wallace, A.J. Fitzgerald, S. Shankar, N. Flanagan, R. Pye, J. Cluff, D.D. Arnone, Terahertz pulsed imaging of basal cell carcinoma ex vivo and in vivo. *Br. J. Dermatol.* **151**, 424–432 (2004)
33. D.M. Mittleman, R.H. Jacobsen, M.C. Nuss, T-Ray Imaging. *IEEE J. Sel. Top. Quantum Electron.* **2**, 679–692 (1996)
34. N. Kukutsu, Y. Kado, Overview of millimeter and terahertz wave application research. *NTT Tech. Rev.* **7**, 1–6 (2009)
35. F.A. Benson, G. Mayo, Effects of ambient-temperature variations on glow-discharge tube characteristics. *J. Sci. Instrum.* **31**, 118–120 (1954)
36. Private communication. <https://www.intl-lighttech.com/specialty-light-sources/neon-lamps>. Cited 13 April 2018
37. W.G. Miller, *Using and Understanding Miniature Neon Lamps* (Howard W. Sams & Co., Inc, Indianapolis, 1969)
38. L. Hou, W. Shi, S. Chen, Z. Yan, Terahertz continuous wave detection using weakly ionized plasma in inert gases. *IEEE Electron Device Lett.* **34**, 689–691 (2013)
39. Y.P. Raizer, *Gas Discharge Physics* (Springer, Berlin, Germany, 1991)
40. E.W. McDaniel, *Collision Phenomena in Ionized Gases* (Wiley, New York, NY, USA, 1964)
41. N. S. Kopeika, J. Rosenbaum, Subnormal glow discharge detection of optical and microwave radiation. *IEEE Trans. Plasma Sci.* **4**, 51–61 (1976)
42. N.S. Kopeika, Noise spectra of commercial indicator-lamp glow-discharge detectors. *Int. J. Electron.* **39**, 209–218 (1975)
43. N.S. Kopeika, N.H. Farhat, Video detection of millimeter waves with glow discharge tubes: part I-physical description; part II-experimental results. *IEEE Trans. Electron Devices* **22**, 534–548 (1975)
44. K. Nanbu, Probability theory of electron-molecule, ion-molecule, molecule-molecule, and coulomb collisions for particle modelling of materials processing plasmas and cases. *IEEE Trans. Plasma Sci.* **28**, 971–990 (2000)
45. S. Longo, Monte carlo models of electron and ion transport in non-equilibrium plasmas. *Plasma Sources Sci. Technol.* **9**, 468–476 (2000)
46. Compilation of electron cross sections used by A. V. Phelps. http://jilawwww.colorado.edu/~avp/collision_data/electronneutral/ELECTRON.TXT. Cited 4 May 2018
47. Phelps database. <http://www.lxcat.net>. Cited 4 May 2018
48. Biagi database (Magboltz versions 8.9 and higher). <http://www.lxcat.net>. Cited 11 April 2018
49. A.V. Phelps, Diffusion, de-excitation, and three-body collision coefficients for excited neon atoms. *Phys. Rev.* **114**, 1011–1025 (1959)
50. A.V. Phelps, J.P. Molnar, Lifetimes of metastable states of noble gases. *Phys. Rev.* **89**, 1202–1212 (1953)
51. W.H. Cramer, Elastic and inelastic scattering of lowvelocity ions: He+ in Ne, Ne+ in He, and Ne+ in Ne. *J. Chem. Phys.* **28**, 688–690 (1958)
52. C. Kusoglu-Sarikaya, H. Altan, D. Akbar, Parallel 1d3v particle in cell/monte carlo collision (PIC/MCC) simulation of a glow discharge millimeter wave detector, in *Proceedings of the 6th International Conference on Photonics, Optics and Laser Technology*, vol. 1 (2018) pp. 110–115

53. H.D. Hagstrum, Auger ejection of electrons from tungsten by noble gas ions. *Phys. Rev.* **104**, 317–318 (1956)
54. H. Bruining, *Physics and Applications of Secondary Electron Emission* (Philips Research Laboratories, Netherlands, Eindhoven, 1954)
55. L.B. Loeb, *Basic Processes of Gaseous Electronics* (University of California Press, California, 1960)